Rodolfo T. Gonçalves
e-mail: rodolfo_tg@tpn.usp.br

André L. C. Fujarra
e-mail: afujarra@usp.br

Guilherme F. Rosetti
e-mail: guilherme.feitosa@tpn.usp.br

Kazuo Nishimoto
e-mail: knishimo@usp.br

TPN–Numerical Offshore Tank,
Department of Naval Architecture and Ocean Engineering,
Escola Politécnica,
University of São Paulo,
Avenue Professor Mello Moraes, 2231,
Cidade Universitária,
São Paulo, SP, 05508-900, Brazil

Mitigation of Vortex-Induced Motion (VIM) on a Monocolumn Platform: Forces and Movements[1]

A great deal of works has been developed on the spar vortex-induced motion (VIM) issue. There are, however, very few published works concerning VIM of monocolumn platforms, partly due to the fact that the concept is fairly recent and the first unit was only installed last year. In this context, a meticulous study on VIM for this type of platform concept is presented here. Model test experiments were performed to check the influence of many factors on VIM, such as different headings, wave/current coexistence, different drafts, suppression elements, and the presence of risers. The results of the experiments presented here are motion amplitudes in both in-line and transverse directions, forces and added-mass coefficients, ratios of actual oscillation and natural periods, and motions in the XY plane. This is, therefore, a very extensive and important data set for comparisons and validations of theoretical and numerical models for VIM prediction.
[DOI: 10.1115/1.4001440]

Keywords: vortex-induced motion (VIM), monocolumn platform, model tests

1 Introduction

Monocolumn, as well as spar platforms, being structures of low aspect ratio, are expected to sufficiently present 3D vortices-emission patterns and a great susceptibility to appendages present at the hull, particularly the fairleads. A brief overview about the relevant aspects of VIM on spar and monocolumn platforms can be found in Ref. [1].

Results indicating these characteristics of VIM on monocolumn platforms have also been presented in works on MonoGoM platform. Further information can be found, among others, in Refs. [2,3].

On the other hand, results reported in this literature demonstrate that these effects are particularly related to the geometry of each unit; therefore, it is difficult to predict the behavior of a unit in a general fashion.

Due to these facts and at the current level of knowledge and development of numerical practices, it is almost imperative to perform scale model tests in order to verify the effects caused by the appendages on VIM of monocolumns.

Hence, the test matrix developed for the present work comprised a series of runs at a physical towing tank in which a reduced-scale model was exposed to several current incidences and VIM mitigation effects.

Section 2 presents, in detail, the experimental setup and tests performed in each case. Section 3 presents the analysis methodology of the experimental results obtained. Section 4 presents the results and their respective discussion. Finally, Sec. 5 presents the conclusions about the extensive experimental work, besides suggestions for further investigation to complement the works conducted so far.

2 Experimental Setup

The experimental setup is characterized by a scale model of the MonoBR floating unit, secured by a set of equivalent horizontal moorings in the towing tank at the Institute of Technological Research (IPT) in São Paulo, Brazil.

The set is towed by the main car of the towing tank, together with the instrumentation dedicated to real-time monitoring of the important physical parameters for the VIM phenomenon, in this case: displacement and accelerations on the *XY* plane (the same as the free surface); forces in each of the four springs that compose the equivalent horizontal mooring and the towing velocity.

2.1 Reduced-Scale Model. The definition of the reduced scale was made based on the geometry of the test basin at the IPT ($4.0 \times 6.6 \times 280.0$ m, respectively, depth $\times$ width $\times$ length). Besides this geometry, the possible velocities that may be developed by the main car of the towing tank were also a determinant factor for the definition of the reduced-scale model. These two factors, together, were important in defining the magnitude of the typical periods of oscillation due to VIM and, therefore, to determine the number of oscillation cycles registered. It is important to outline that the reduced scale researched would have to allow for a greater number of complete oscillation cycles due to VIM as a way to characterize the monitored parameters as much as possible.

The ratio between the reduced-scale diameter and the width of the model test basin was also considered in order to avoid scale effects and mainly proximity with the side walls of the tank, which could interfere with the results of interest.

The adopted scale was 1:200. The magnitude of the monitored parameters was also taken into account in order to avoid an excessive reduction in the dimensions of the model.

The main dimensions of the MonoBR are presented in Table 1. The detailed geometry of the platform, including the hydrodynamical appendages for heave reductions, is presented in Fig. 1. More information on the appendages can be seen in Ref. [4].

As presented in Fig. 2, the Reynolds numbers effectively used in the experiments are within the range of 0.5×10^5 to 2.0×10^5, which do not represent the flow condition in real scale. In fact, such compatibility would be impossible in the model test tank, due to its dimensions and also because of the possible velocities of the main car of the towing tank.

As a usual alternative, a strategy to induce postcritical flow

[1]This paper includes OMAE2009-79380: "Mitigation of Vortex-induced Motions of a Monocolumn Platform," presented in the 28th International Conference on Ocean, Offshore and Arctic Engineering, 2009, Honolulu, HI, and new results about forces due to the VIM.

Contributed by the Ocean Offshore and Arctic Engineering Division of ASME for publication in the JOURNAL OF OFFSHORE MECHANICS AND ARCTIC ENGINEERING. Manuscript received September 22, 2009; final manuscript received February 3, 2010; published online September 24, 2010. Assoc. Editor: Sergio Sphaier.

Table 1 Main characteristics of the unit

Diameter at the bottom	138.60 m
Characteristic diameter	108.00 m
Depth	55.00 m
Low draft test	23.00 m
Full draft test	42.00 m
Displacement in low draft	220,000 tons
Displacement in high draft	372,000 tons

regime was adopted by the inclusion of controlled surface roughness to the model. The definition of the roughness level was based on the work of Allen and Henning [5], in which the behavior of the drag coefficient was observed for each level of surface roughness, all coefficients being a function of the Reynolds number. According to the analysis conducted by Allen and Henning [5], by means of monitoring the drag coefficient, a minimum level of surface roughness can be defined so that the reduced scale presents a flow regime similar to the real condition, therefore, postcritical.

The roughness value of $k/D=4.0\times10^{-3}$ utilized in this experiment was first suggested by van Dijk et al. [6], and used later in a MonoGoM VIM study, from which a reasonable result was presented, as can be observed in Ref. [2].

Figure 3 shows a detailed picture of the surface roughness added to the reduced-scale model. Also according to this figure, the presence of the fairleads is noted and they are the only appendages with hydrodynamical importance; thus, they were maintained in the modeling of the MonoBR platform in reduced scale. Figure 4 presents a picture of the complete model of the platform.

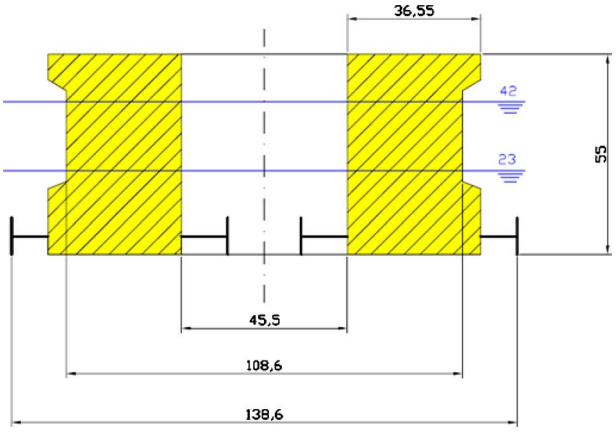

Fig. 1 Sketch of the main dimensions of the unit

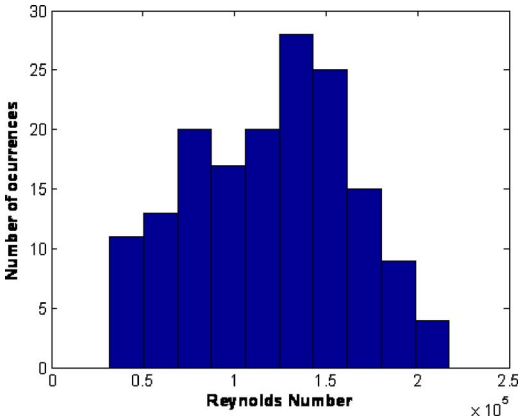

Fig. 2 Plot presents the range of Reynolds numbers that were tested

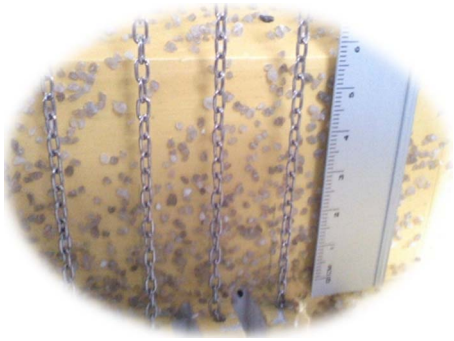

Fig. 3 Roughness of the model in detail ($k/D=4\times10^{-3}$)

2.2 Equivalent Mooring. In relation to the mooring system, although its real configuration of the MonoBR platform is characterized by the presence of three groups of moorings, this arrangement showed a larger susceptibility to the nonlinear restoring forces, mainly in large offset situations (typical in flows of large velocity).

According to Gonçalves et al. [3] the equivalent mooring with four springs showed to be more linear than the equivalent mooring with three springs, contributing to a more controlled motion of the unit (a larger time in regime). The equivalent mooring with four springs was adopted as it also showed to be more practical concerning the exchange of heading and calibration of the stiffness constant. A schematic drawing of the mooring system is presented in Fig. 5.

Table 2 presents the geometry of the experiments in detail and the spots where the lines are moored on the model and on the towing car. The coordinates of the initial mooring point of spring i are (x_{0i},y_{0i},z_{0i}), the coordinates of the platform mooring point of spring i at the initial instant $(t=0)$ are (x_i,y_i,z_i), and $Z=0$ represents the water line level.

2.3 Test Matrix. The purpose of this test was to complete the studies of monocolumn VIM initiated in Ref. [2]. By making use of published works in literature about the study of spar and monocolumn VIM, a battery of tests was performed so as to verify the influence of certain characteristics. They are listed as follows.

- *Heading.* In spar, a large sensitivity of the VIM phenomenon was verified according to the direction of flow, as can be observed in Refs. [7–9]. In monocolumn platforms, this effect was only studied for two heading conditions, see Ref. [3], which increases the importance of the tests on a larger number of headings.
- *External appendages of the hull.* They can significantly

Fig. 4 Picture of the model made with polyvinyl chloride (PVC)

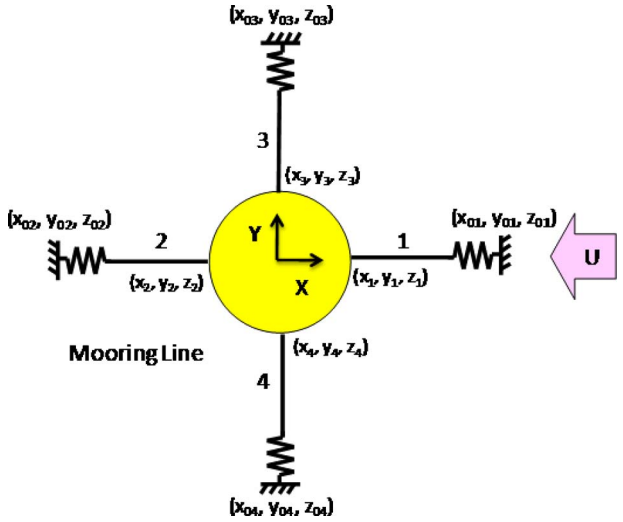

Fig. 5 Sketch of the equivalent mooring system composed of four lines

change the flow around the hull, as seen in Refs. [10,7,11].

- *Motion suppressor.* The presence of a strake type motion suppressor on a spar showed to be efficient, as can be seen in Refs. [12,6,13]. The results of the use of suppressors (spoiler plates) on monocolumn platforms also showed to be efficient, according to Gonçalves et al. [3]; therefore, it is important to analyze other configurations of spoiler plates;
- *Concomitant presence of wave and current.* The spar works performed by van Dijk et al. [31] and Irani and Finn [13] showed the need to study VIM in the presence of waves. The work of Finningan et al. [14] was the first to show the results of VIM in the presence of waves, which makes the study interesting for monocolumn platforms;
- *External damping.* The works performed by van Dijk et al. [31] and Yung et al. [15] showed the importance of including external damping—for example, due to risers—in the tests. Therefore, a battery of tests studied this matter.
- *Light weight condition.* In the work of Fujarra et al. [16], the results of VIM of the monocolumn platform SSP Piranema were published and it was verified that they were very different from those of the MonoGoM in Ref. [2]. The reason can be attributed to the difference between the immersed portions of each unit; thus the need of analyzing different drafts becomes evident.

Due to the concerns mentioned before, a test matrix capable of including all these factors was elaborated. Hence the test matrix includes the following.

- *Five conditions of heading.* Each heading with its respective equivalent mooring. The equivalent mooring was determined as the procedure showed in Ref. [2], which considered each condition of ambiental incidence.
- One condition with the presence of spoiler plates.

Table 2 Configuration of the mooring for the full draft tests

Mooring line ID	x_{0i} (mm)	y_{0i} (mm)	z_{0i} (mm)	x_i (mm)	y_i (mm)	z_i (mm)
1	3300	0	430	345.5	0	−185
2	−3300	0	430	−346.5	0	−185
3	0	1500	520	0	346.5	−185
4	0	−1500	520	0	346.5	−185

Table 3 Test matrix

Test	Heading (deg)	Draft	Appendages	Extras
Heading	0	Full	Fairleads and chains	-
	45	Full	Fairleads and chains	-
	135	Full	Fairleads and chains	-
	180	Full	Fairleads and chains	-
	315	Full	Fairleads and chains	-
Waves	0	Full	Fairleads and chains	With regular waves
Spoiler plates	0	Full	Fairleads, chains, and spoiler plates	-
External damping	0	Full	Fairleads and chains	-
Draft	0	Low	Fairleads and chains	-

- One condition with external damping due to the presence of risers.
- One condition with the presence of waves and current.
- One condition with light draft.

The test matrix is presented in detail in Table 3. In previous monocolumn tests, see Ref. [3], the range of the Vr_n tests was small and limited, most of the times to $Vr_n < 12$. The tests presented in this work were planned so as to include a range of $3 < Vr_n < 15$ and with a discretization of at least 18 velocities.

3 Analysis Methodology

The standard procedure used for the analyses of the results was proposed by Gonçalves et al. [3], and the most important points are rewritten in this section.

3.1 Nondimensional Motion Amplitudes. The value of A_Y/D is defined as the average of the 20% highest peaks of the motion signal due to the reduced number of peaks, instead of the usual 10% found in the vortex-induced vibration (VIV) literature. Hence,

$$A_Y/D = \frac{\sum_{i=1}^{1/5n} |Y_i|}{\frac{1}{5}n} \tag{1}$$

where Y_i is the value of the ith peak amplitude, the peaks are ordered from the highest to the lowest with Y_1 being the highest of all peaks, and n representing the number of peaks of the motion signal.

3.2 Hydrodynamic Forces. The linear rigid body motion equations for a platform with two uncoupled degrees of freedom (DOFs) are represented by Sarpkaya [17] as follows:

$$m\ddot{Y}(t) + C\dot{Y}(t) + K_y Y(t) = F_{Hy}(t) \tag{2}$$

$$m\ddot{X}(t) + C\dot{X}(t) + K_x X(t) = F_{Hx}(t) \tag{3}$$

where m represents the platforms mass, C is the structural damping coefficient of the system, and F_{Hy} and F_{Hx} are the total hydrodynamic forces acting on the system in the x and y directions.

In the experiments, the total hydrodynamic forces in each given direction are measured indirectly using these motion equations. The total hydrodynamic force is the sum of the inertial, dissipative, and restoring forces of the system. Preliminarily, the structural dissipative force (structural damping) can be disregarded,

considering it has a smaller magnitude value than the other forces involved in the system dynamics. Therefore, the hydrodynamic force is obtained by the sum of the restoring and inertial forces.

In this way, the force in the transverse direction to the flow (y, transverse direction) is commonly represented in the form of the nondimensional lift coefficient C_L, as in

$$F_{Hy}(t) = \tfrac{1}{2}\rho S U^2 C_L(t) \tag{4}$$

$$C_L(t) = \frac{2F_{Hy}(t)}{\rho S U^2} \tag{5}$$

where ρ is the fluid density, S is the submerged projected area of the platform in relation to the transverse direction to the flow, and U is the flow speed.

The force in the parallel direction to the flow (x, in-line direction) can be divided into two parts: one related to the average drag force (static component) and a second one related to the dynamic drag force (oscillatory component). Thus, the average part of the drag can be described as

$$\overline{F_{Hx}(t)} = \tfrac{1}{2}\rho S U^2 C_D \tag{6}$$

$$C_D = \frac{2\overline{F_{Hx}(t)}}{\rho S U^2} \tag{7}$$

where $\overline{F_{Hx}(t)}$ is the average total hydrodynamic force in the in-line direction and C_D is the average drag coefficient.

The oscillatory component can be described as

$$F_{Hx}(t) - \overline{F_{Hx}(t)} = \tfrac{1}{2}\rho S U^2 C_{Dd}(t) \tag{8}$$

$$C_{Dd}(t) = \frac{(2F_{Hx}(t) - \overline{F_{Hx}(t)})}{\rho S U^2} \tag{9}$$

where $C_{Dd}(t)$ is the dynamic drag coefficient.

Therefore, assuming an approximately harmonic VIM response, the total hydrodynamic force in the transverse direction can be described, as presented in Refs. [18,17] as

$$F_{Hy}(t) = F_0 \sin(\omega t + \emptyset) = F_0 \cos \emptyset \sin \omega t + F_0 \sin \emptyset \cos \omega t \tag{10}$$

where F_0 is the total hydrodynamic force amplitude in the transverse direction, ω is the angular frequency of the motion, and $\emptyset$ is the phase between force and motion.

This fluid-originated force can be divided into two components: one in phase with the platform acceleration and the other in phase with the platform velocity. In this way, the nondimensional lift coefficient can be stated as

$$C_L(t) = C_a \sin \omega t - C_{Dy} \cos \omega t \tag{11}$$

where C_a is an "effective" added-mass coefficient that includes an apparent effect due to the total transverse fluid force in phase with the body acceleration, introduced by Khalak and Williamson [19] and reviewed by Sarpkaya [17], and C_v is a damping that includes the total transverse fluid force in phase with the body velocity (e.g., hydrodynamic viscous damping and pressure force).

In a less susceptible manner to the monochromatic harmonic character, Fujarra and Pesce [20] proposed a classical analysis on the frequency domain for estimating the added-mass coefficient.

According to that analysis, the following relation can be stated:

$$\frac{\mathcal{F}[F_{Hy}(t)]}{\mathcal{F}[\ddot{Y}(t)]} \approx -m_a(\omega) + \frac{iC_{Dy}(\omega)}{\omega} \tag{12}$$

where $\mathcal{F}[\ ]$ is the Fourier transform of the signal, m_a is the added mass, and C_v is the viscous damping coefficient.

Therefore,

$$C_a^{FD} = C_a^{FD}(\omega) = \frac{-\Re\left\{\dfrac{\mathcal{F}[F_{Hy}(t)]}{\mathcal{F}[\ddot{Y}(t)]}\right\}}{m} \tag{13}$$

where $\Re[\ ]$ is the real part of the complex number resulting from the analysis through the Fourier transform.

In this case, the added-mass coefficient is calculated for each motion frequency, allowing the identification only of the force contribution on the frequency of interest (dominant on the registry).

3.3 Reduced Velocities. The reduced velocity is defined for each drift level, taking into account the eventual alteration on the added mass and stiffness; thus

$$Vr_n = \frac{UT_n}{D} \tag{14}$$

where T_n is the natural period of the motion on the new drift condition and flow speed, calculated as

$$T_n = 2\pi\sqrt{\frac{(1 + C_a)m}{K_y}} \tag{15}$$

This definition of Vr_n shows to be more coherent with the parameters that dictate the system in a given fluid-structure interaction, and therefore, it is more representative in relation to the VIM phenomenon, as also noted in Ref. [13].

4 Results

In this section, some of the most important results of the analysis on the phenomenon of VIM will be presented.

For the presentation of the results, nondimensional values were always adopted, which is the usual practice in studies of the phenomenon of fluid-structure interaction. Therefore, we have the following.

- For the results of the response amplitude in the in-line direction the nondimensional A_x/D was adopted, where A_x refers to the amplitude motion in the in-line direction and D refers to the characteristic diameter of the floating unit.
- Similarly, for the results of response amplitude in the transverse direction, the nondimensional A_y/D was adopted, where A_y refers to the motion amplitude in the transverse direction of the incident flow.
- Referring to periodicity, for the ratios of oscillation periods in each direction, in-line and transverse, and the natural period in the transverse direction, the nondimensional values T_x/T_{ny} and T_y/T_{ny} were adopted.
- With regard to forces, the usual hydrodynamic nondimensional quantities were adopted, thus, C_D for the medium drag, C_{Dd} for the dynamic drag superposed to the medium drag, C_L for the lift, and C_a for the added mass.
- The results of combined motion on the XY plane are presented. These results are plotted in polar diagrams and represent what really occurred with the platform subjected to VIM.

4.1 Tests With Change in Heading. The first tests aimed at the verification of the influence of the hull appendages—particularly the fairleads—on the response of the MonoBR VIM.

Parallel to this, it was useful to solidify the experimental procedures and, at the same time, determine an extreme behavior, referred to as a base case, in which mitigation elements acted.

Therefore, the discussion of the results is initiated by presenting nondimensional amplitudes as the function of reduced velocity for the 0-deg incidence; see Fig. 6. It is possible to note that in both in-line and transverse directions the results were rather repetitive. In relation to the repeatability of results, it is important to outline that maximum attention was paid to the apparatus and to the test

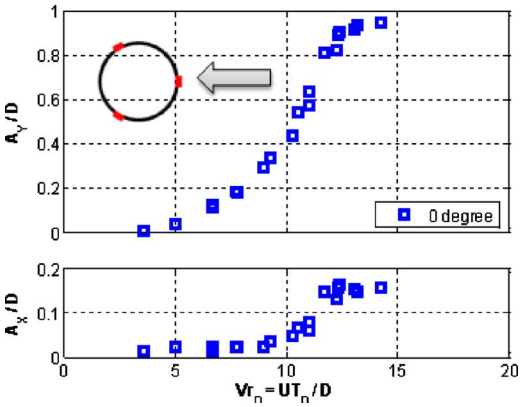

Fig. 6 Variation of the nondimensional amplitudes as a function of the reduced velocities for the 0-deg incidence

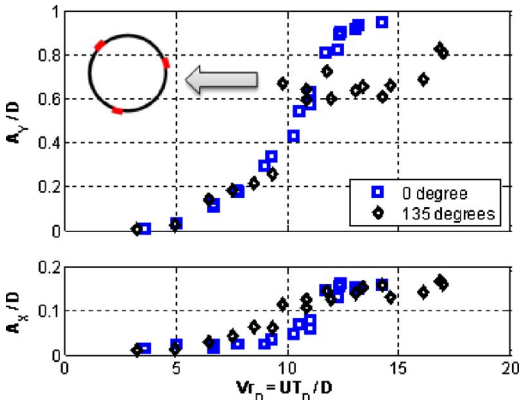

Fig. 8 Variation of the nondimensional amplitudes as a function of the reduced velocities for the 135-deg incidence

procedures. Still in Fig. 6, it is possible to note that large motions in $Vr_n > 5$, attaining $A_y/D \cong 0.95$ and $A_x/D \cong 0.15$ in around $Vr_n = 14$. It is important to note that large amplitudes of the motion in the transverse direction come from the coexistence with the motion in the in-line direction, as widely discussed in literature; see Refs. [21–23].

It is interesting to note as well that, when the motion in the in-line direction seems to grow, i.e., as $Vr_n = 11$, the transverse response seems to have a distinct branch (superupper branch as denominated by Stappenbelt and Lalji [23]), possibly associated with coexistence with the in-line oscillations. Such a fact can only be confirmed by measuring the flow velocity around the body and, therefore, identifying a distinct vortex emission pattern.

Continuing the discussion, Figs. 7–10 demonstrate the comparison between various tested incidences. In general, it is evident that the change in the heading and, therefore, in the relative position of the appendages, causes significant alterations on the motion in the transverse direction for the large reduced velocities, $Vr_n > 11$.

The 45-deg, 135-deg, and 315-deg incidences show an evident decrease in the motion in the transverse direction. This fact may be related to the decrease in emission correlation and, therefore, a weaker interaction between the motion in both in-line and transverse directions.

Concerning the 0-deg and 180-deg incidences, in the range of $5 < Vr_n < 11$, there is not a very large difference in terms of amplitudes. For $Vr_n > 11$, there is an abrupt decrease in the amplitudes. This possibly happens due to the fact that the point where the boundary layer separates it moves around the hull with the increasing velocities and, when in reaches 60 deg from the bow of the platform, the separation point is fixed in both fairleads. Therefore, for $Vr_n > 11$, vortices are shed prematurely and the vortex street is less uniform and correlated causing this decrease in motion amplitudes.

However, this is not true in the range of $5 < Vr_n < 11$. In this range, it is not possible to note a large influence of the heading on the VIM response, which is of some concern, as it is the range of the real current.

In terms of the ratio between the periods of oscillation, independently of the incidence, it is possible to note that, in the ranges of important oscillations, $Vr_n > 11$, the values are not altered with the change in the heading. Such behavior is seen in Figs. 11–14,

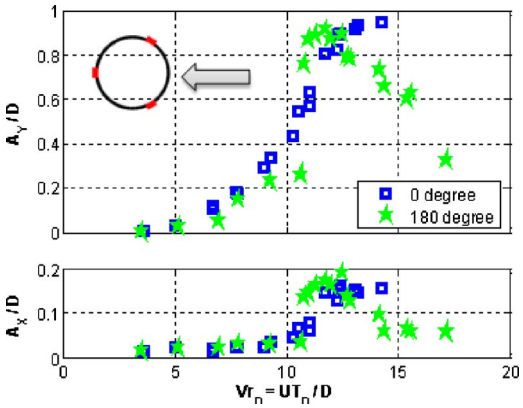

Fig. 9 Variation of the nondimensional amplitudes as a function of the reduced velocities for the 180-deg incidence

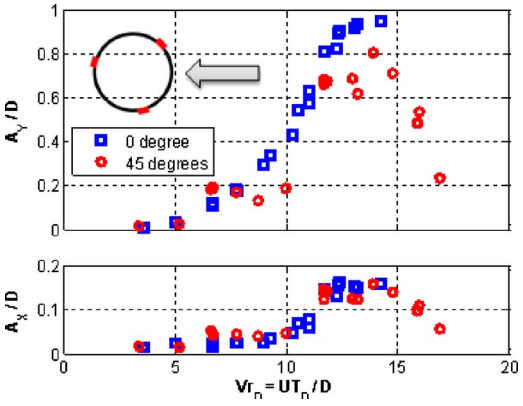

Fig. 7 Variation of the nondimensional amplitudes as a function of the reduced velocities for the 45-deg incidence

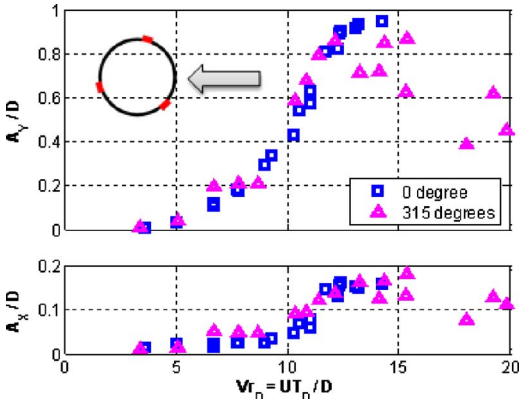

Fig. 10 Variation of the nondimensional amplitudes as a function of reduced velocities for the 315-deg incidence

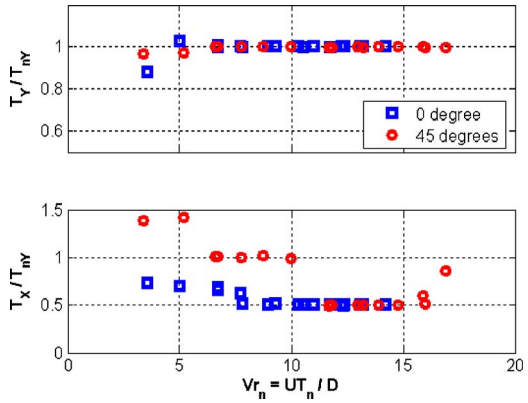

Fig. 11 Variation of the nondimensional periods as a function of the reduced velocities for the 45-deg incidence

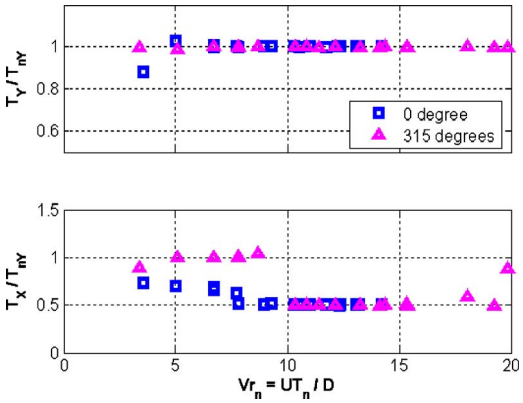

Fig. 14 Variation of the nondimensional periods as a function of the reduced velocities for the 315-deg incidence

where nondimensional periods of oscillation are presented.

On the other hand, in the range of $5 < Vr_n < 11$, dispersion in the values of in-line period ratios can be seen, $T_x/T_{ny} < 1.5$. This is related to the fact that, in this range, the amplitudes of motion in the in-line direction present small values, in such a way that it becomes difficult to characterize the typical periodicity.

In general, whenever simultaneous motions in the in-line and transverse directions were present, it was possible to identify $T_y/T_{ny} \cong 1.0$ and $T_x/T_{ny} \cong 0.5$. In fact, this behavior implies a remarkable feature of motion trajectories seen on the *XY* plane. An interesting way to visualize the periodicity discussed before is presented in Fig. 15, which presents the typical motion trajectories and the flow velocity. Together with the increase in velocity, the motions in the transverse direction increase. From $Vr_n = 11$, it is possible to observe that the motion in the in-line direction rises, originating eight-shaped trajectories. Other examples of the eight-shaped trajectory can be found in Refs. [21,24]. The black circle in the center of the plot indicates the platform with the relative positions of the fairleads (square marks). Furthermore, each of the trajectories has its dynamic equilibrium point correctly spaced from the zero in-line equilibrium point (center point of the diagram).

In Figs. 16 and 17, the trajectories for the other incidences are presented. Note that, according to Figs. 7–10, the other headings present smaller maximum amplitudes than for the 0-deg incidence. In some cases, the eight-shaped trajectory is even nonsymmetric (see, e.g., 135-deg incidence in Fig. 17(*b*)).

Figure 18 presents the results of the drag coefficients for the 0-deg incidence. According to these results, $C_D \cong 0.7$ for $Vr_n < 11$; and, for $Vr_n > 11$, the presence of dynamic amplification of drag is verified. In this region, the value of the medium drag coefficient is higher, $C_D \cong 0.9$, which corresponds to the increase in nondimensional amplitudes due the simultaneous presence of

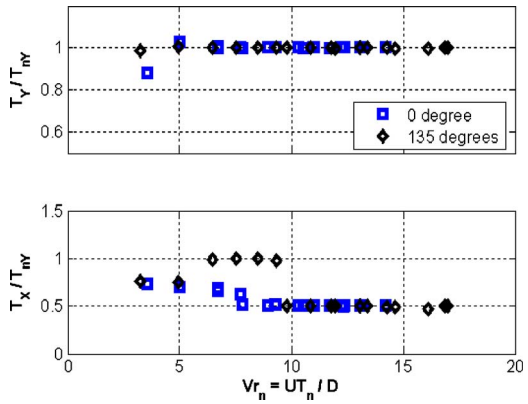

Fig. 12 Variation of the nondimensional periods as a function of the reduced velocities for the 135-deg incidence

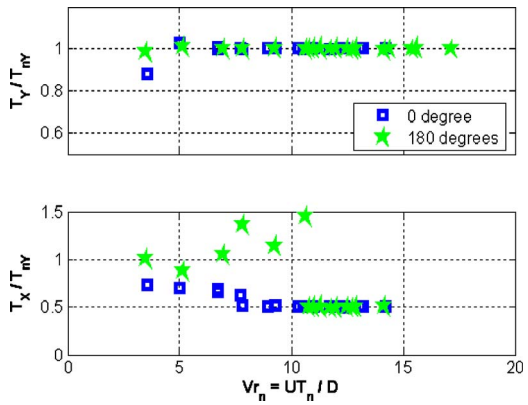

Fig. 13 Variation of the nondimensional periods as a function of the reduced velocities for the 180-deg incidence

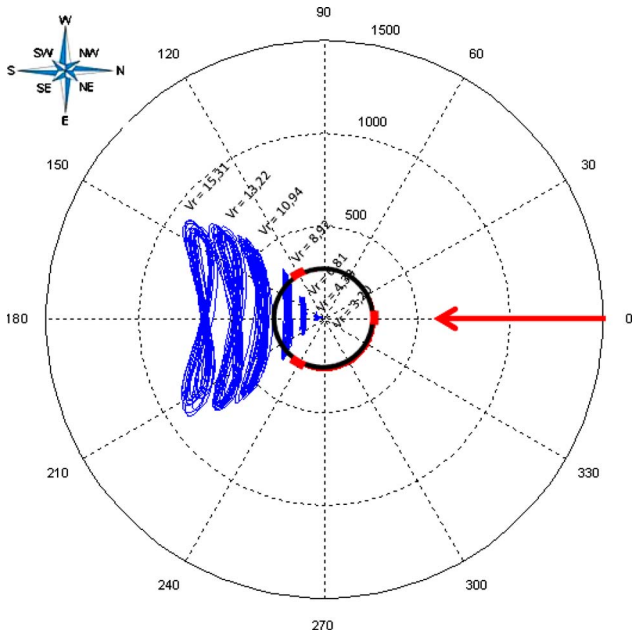

Fig. 15 Motion on the *XY* plane for the 0-deg incidence

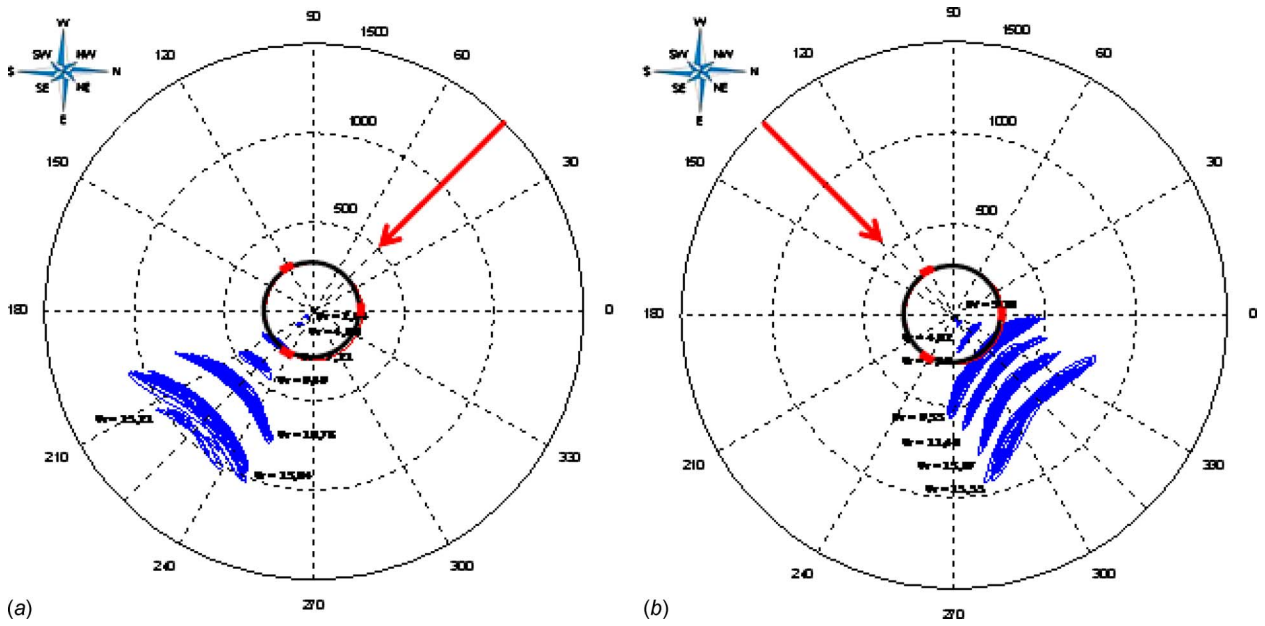

Fig. 16 Motion on the *XY* plane for the (*a*) 45-deg and (*b*) 135-deg incidences

motions in both transverse and in-line directions.

Regarding the dynamic drag, it is verified that values of $C_{Dd} \cong 0.05$ for the range of $5 < Vr_n < 11$ were obtained, as well as $C_{Dd} \cong 0.10$ outside this range. The larger motion in the in-line direction is responsible for this change (dynamic amplification).

Figures 19–22 present the results of the drag coefficients for the 45-deg, 135-deg, 180-deg, and 315-deg incidences, respectively. In particular, the results for C_D and C_{Dd} are higher for the 180-deg incidence. The reason is the larger nondimensional amplitude of oscillation in the range $11 < Vr_n < 13$, and the dynamic amplification of drag is present again in this case. No significant modifications are found in the other incidences.

Figure 23 presents the results for the lift C_L and for the added mass C_a coefficients for the 0-deg incidence. According to these results, the value for C_L increases up to $Vr_n = 11$ and decreases gradually above this reduced velocity. The result confirms that the large motion in the transverse direction for $Vr_n > 11$ is not associated with the continuous increase in the lift coefficient acting under the platform, but it is associated with the coexistence of the motion in both directions, characterized by the eight-shaped figure.

It is interesting to note that the C_a has a constant value $C_a \cong 1.2$, up to $Vr_n \cong 10$, and the value decreases quickly from this reduced velocity, when there is coexistence of the motion in both directions.

The C_L for the other incidences, Figs. 24–27 (45-deg, 135-deg, 180-deg, and 315-deg, respectively), is not possible to identify a distinct behavior compared with the results for 0-deg incidence. The important point is the value of $C_L \cong 0.4$ for the maximum lift at all incidences, in $Vr_n \cong 10$.

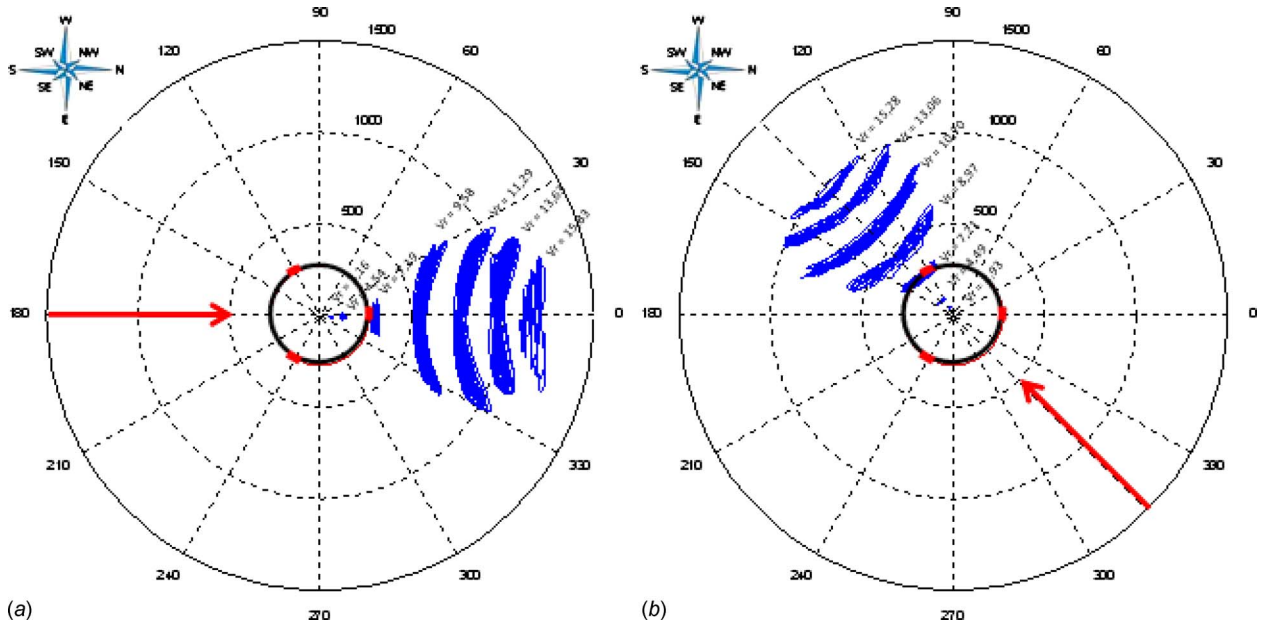

Fig. 17 Motion on the *XY* plane for the (*a*) 180-deg and (*b*) 315-deg incidences

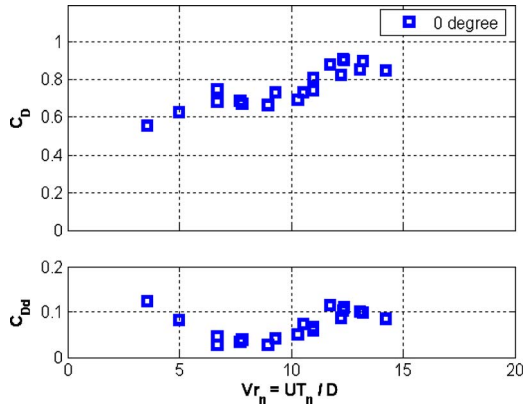

Fig. 18 Variation of drag coefficients as a function of reduced velocities for the 0-deg incidence

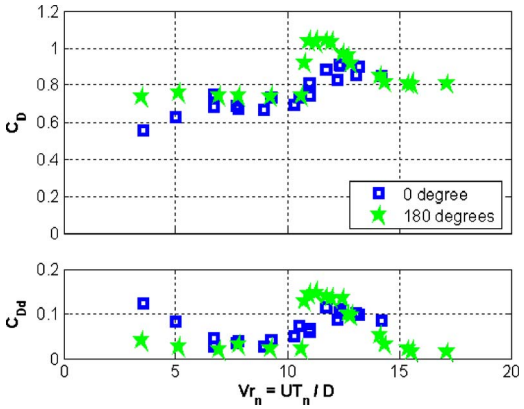

Fig. 21 Variation of drag coefficients as a function of reduced velocities for the 180-deg incidence

As to C_a, the results for the 45-deg, 135-deg, and 180-deg incidences do not present decreasing values in the range $Vr_n > 10$. The behavior is possibly related to low motion amplitudes found in these cases. The increase in the motion in the transverse direction is associated with the decrease in the added inertial force contribution; see, for example, Refs. [25,17].

4.2 Tests With Spoiler Plates. When the tests of the MonoGoM were performed in 2005, a new class of suppressor of innovative geometry was tested aiming to attenuate VIM effects. At the time, spoiler plates, fixed on the side walls of the model placed in three helicoids in the direction of the bottom, showed to be much more efficient in mitigating VIM amplitude. More details can be found in, e.g., Ref. [2].

Following the same investigative direction in the present test campaign, similar geometry was also tested, now with the MonoBR. Figure 28 illustrates this configuration. Albeit similar, the new geometry was altered due to the different shapes of the MonoBR, as compared with the MonoGoM. This, in a way, provided substantially different results presented ahead in this work.

In a preliminary way, Figs. 29 and 30 allow verifying two as-

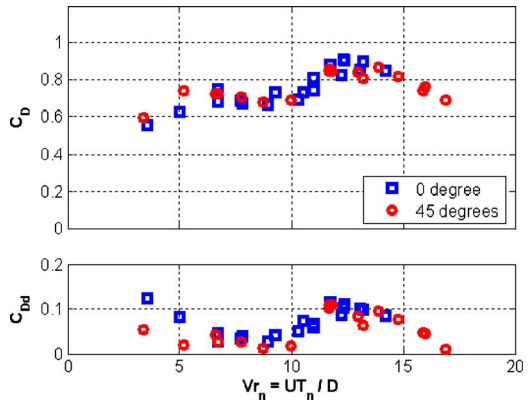

Fig. 19 Variation of drag coefficients as a function of reduced velocities for the 45-deg incidence

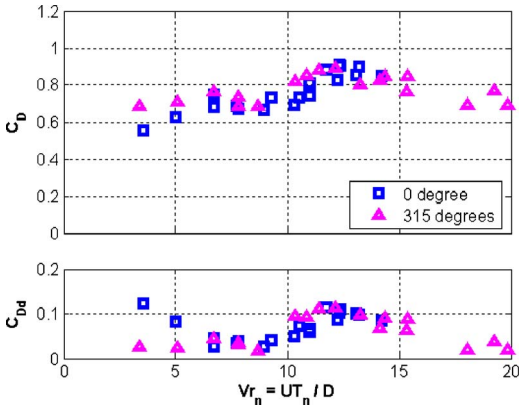

Fig. 22 Variation of drag coefficients as a function of reduced velocities for the 315-deg incidence

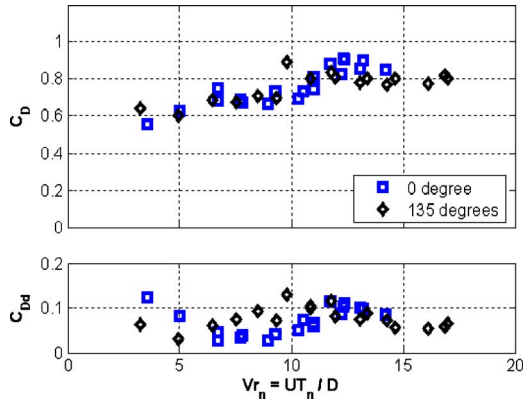

Fig. 20 Variation of drag coefficients as a function of reduced velocities for the 135-deg incidence

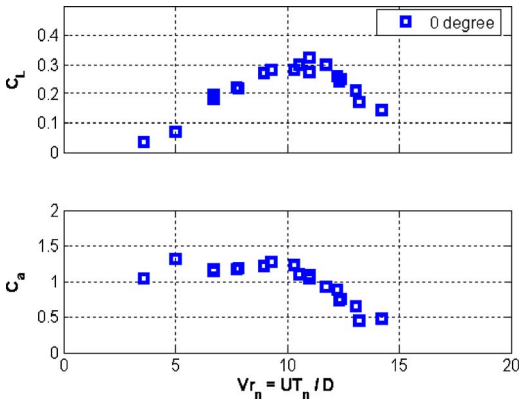

Fig. 23 Variation of the lift coefficient (C_L) above, and the added (C_a) below, as a function of the reduced velocity for the 0-deg incidence

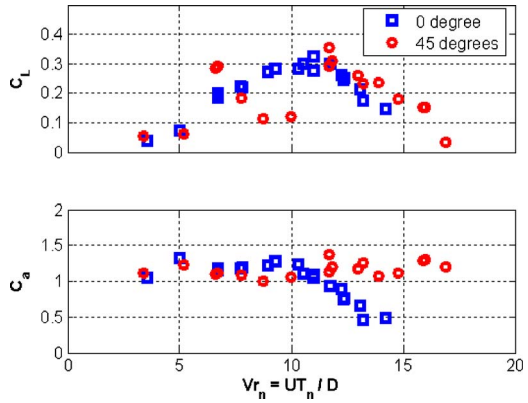

Fig. 24 Variation of the lift coefficient (C_L) above, and the added (C_a) below, as a function of the reduced velocity for the 45-deg incidence

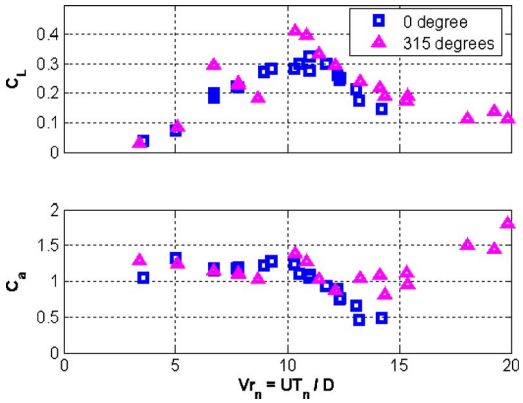

Fig. 27 Variation of the lift coefficient (C_L) above, and the added (C_a) below, as a function of the reduced velocity for the 315-deg incidence

pects of the presence of spoiler plates. Following the intentions established at first, it is possible to note that the presence of such elements causes the reduction in the VIM intensity, mainly in high current values, $Vr_n > 10$. However, in the range of $5 < Vr_n < 10$, the motions in the transverse direction present a small increase in amplitude, possibly related to a simultaneous increase in the motion in the in-line direction. Besides this aspect, it is clear that the ratio of periods of oscillation and the natural cross-flow period present a unitary value differently to the usual ratio of $T_x/T_{ny} \cong 0.5$.

An important difference between the behavior of the MonoBR without the spoiler plates and with them concerns the trajectories on the *XY* plane. According to Fig. 31, it is possible to note that suppressor elements placed in double helicoids along the depth account for rather nonsymmetric trajectories. Furthermore, it is evident that the presence of suppressor elements causes the trajectories to be less coordinated, clearly corresponding to the effect imposed on the wake, which is possibly more influenced by tridi-

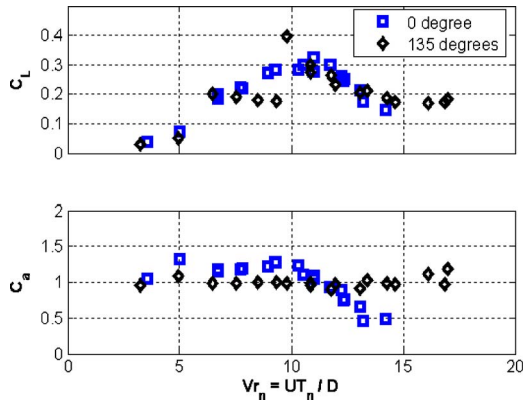

Fig. 25 Variation of the lift coefficient (C_L) above, and the added (C_a) below, as a function of the reduced velocity for the 135-deg incidence

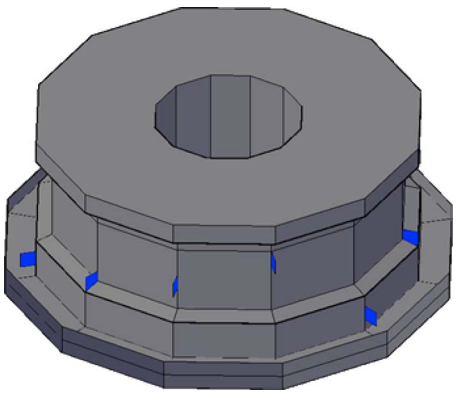

Fig. 28 Sketch of the distribution of the spoiler plates at the monocolumn

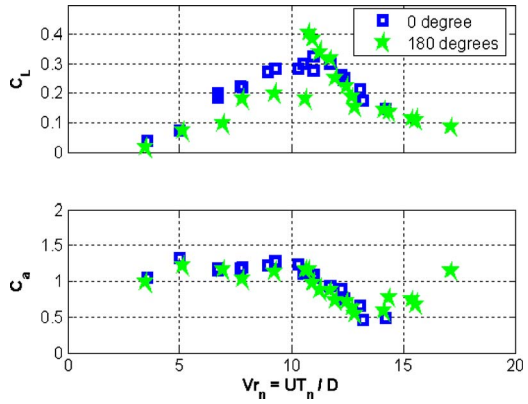

Fig. 26 Variation of the lift coefficient (C_L) above, and the added (C_a) below, as a function of the reduced velocity for the 180-deg incidence

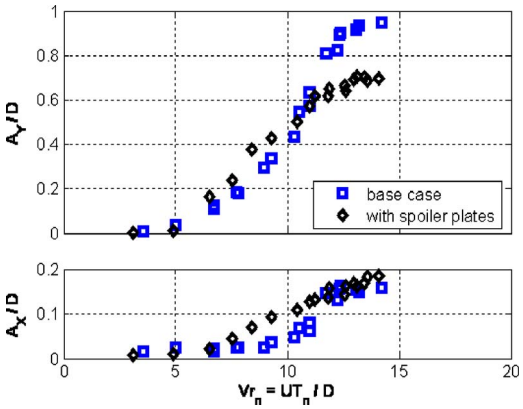

Fig. 29 Variation in the nondimensional amplitudes as a function of the reduced velocity for the 0-deg incidence in the presence of spoiler plates

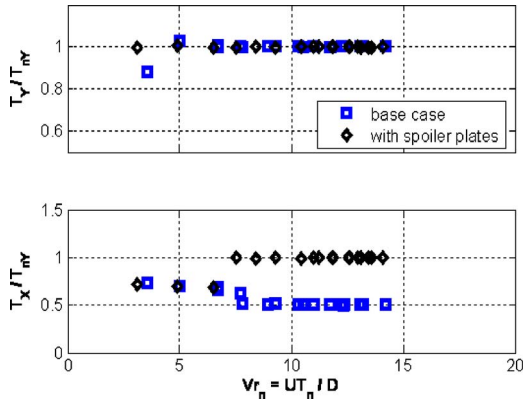

Fig. 30 Variation in the nondimensional periods as a function of the reduced velocity for the 0-deg incidence in the presence of spoiler plates

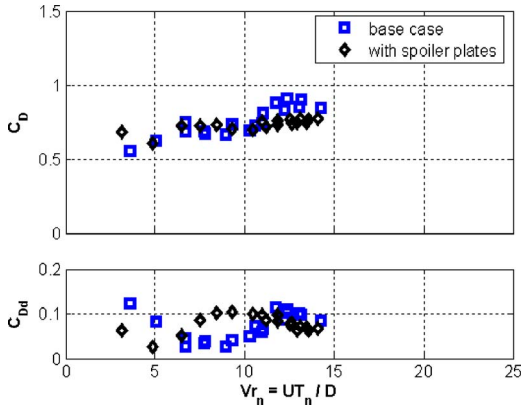

Fig. 32 Variation of drag coefficients as a function of reduced velocities for the 0-deg incidence in the presence of the spoiler plates

mensional effects.

The results for C_D and C_{Dd} in the presence of the spoiler plates, Fig. 32, are not very different if compared with these of the platform without the spoiler plates. The values of C_L in the presence of the spoiler plates, Fig. 33, are smaller than the values without the presence of spoiler plates; it is consistent with the small motion amplitudes observed for $Vr_n > 10$ in this case. The C_a behavior is similar in both cases (with and without the presence of spoiler plates).

4.3 Tests With the Increase in the Damping. The simultaneous presence of risers is surely another aspect, which interferes with VIM response. It is, therefore, a subject that deserves further investigation, particularly, under two points of view. The first concerns the change in the emission pattern near the platform, hence the change in the hydrodynamic forces. The second refers to the inevitable drag increase, which has an important effect on the damping imposed on the structure.

A structural set of risers was built in the model in a similar way to that of a MonoBR (in diameter and positions); however, with only enough length to guarantee the following:

- maintenance of coherence in the emission pattern near the platform
- a known increase in damping, however, not aiming at scaling the real values; see Fig. 34

From Table 4, it can be verified that the quadratic drag coefficient doubles in the configuration with risers, when compared with the value for the hull without it. The quadratic damping coefficient was obtained as proposed in Ref. [26]. This difference represents the increase in damping due to the use of risers. This result is coherent and shows that an increase in the exposed area actually results in an increase in quadratic damping of viscous origin.

Figures 35 and 36 present the VIM response (in terms of nondimensional amplitudes and periods) of the platform in a 0-deg incidence. It also compares the base case with that with the risers. According to this figure, dissipative forces cause a considerable decrease in the motions in the in-line and transverse directions.

It is possible, however, that an increase in dissipation is not the only cause of this behavior. One can speculate that part of such an

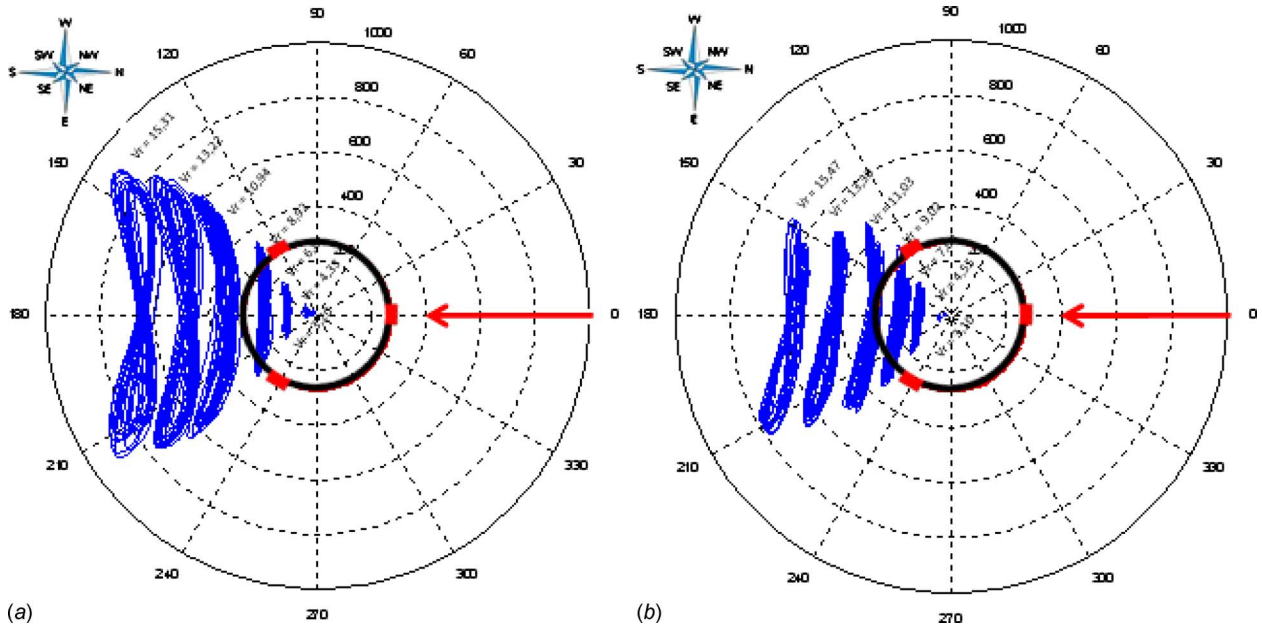

Fig. 31 Motions on the *XY* plane (in-line and cross-flow) for the 0-deg incidence; (*a*) with and (*b*) without presence of spoiler plates

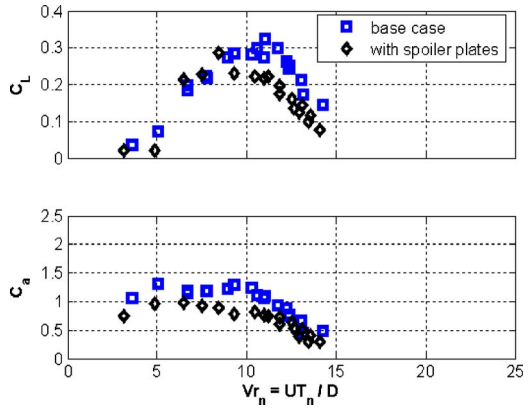

Fig. 33 Variation of the lift coefficient (C_L) above, and the added (C_a) below, as a function of the reduced velocity for the 0-deg incidence in the presence of the spoiler plates

effect caused by the presence of the risers is related to the change in the flow in the surroundings of the platform, which may have been more influenced by tridimensional effects. The loss in correlation may have occurred along the longitudinal dimension of the body. Given the low aspect ratio, the unit becomes extremely susceptible to tridimensional effects (fact observed in a light draft configuration). Hence, a nonhomogeneous distribution of forces along the length causes a smaller resultant force and, therefore, a smaller motion.

Concerning the nondimensional periods, the effects of the presence of risers are noted because of the loss of the ratio $T_x/T_{ny}=0.5$. The absence of the double period ratio has a clear effect over the trajectories. The eight-shaped trajectory is no longer present. Figure 37 illustrates this fact and also allows noting that larger offsets occur. This is coherent with this increase in the quadratic damping coefficient. In this case, contrary to the results from the MonoBR with the spoiler plates, the symmetry of the trajectories was kept.

The results for the drag coefficients, Fig. 38, were affected by the presence of risers. The presence of the risers caused an increase in the value for C_D, as expected, and the low values for C_{Dd}, in the range of $V_r>11$, were due to the absence of the motion in the in-line direction.

The results for C_L, Fig. 39, followed the expected behavior, i.e., smaller values than the base case, whereas the motion amplitudes were smaller. Also, the results for C_a, Fig. 39, were very different

Table 4 Quadratic drag coefficient in the in-line and cross-flow directions for the 0-deg incidence: comparison between the different mitigation propositions

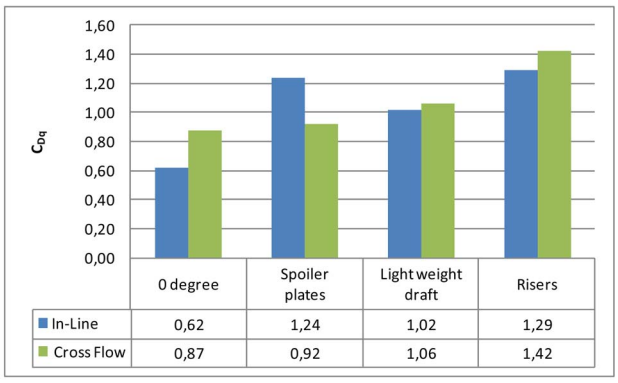

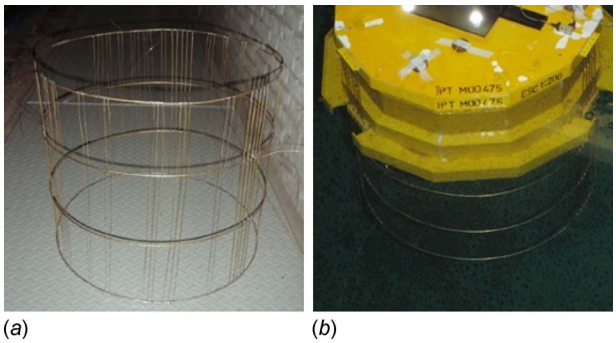

Fig. 34 Complementary distribution of the risers incorporated to the MonoBR, with (*a*) only the risers and (*b*) with the entire set

if compared with the base case, presenting a great dispersion of results. This occurs because high 3D effects are promoted by the device utilized to simulate the external damping.

4.4 Tests With Simultaneous Presence of Waves. The 0-deg incidence was selected as a basis for comparison due to the fact that it is the most responsive condition. In order to better understand the phenomenon (and the mitigation of VIM), regular state sea was chosen, which means that the excitation will be monochromatic. Three regular waves were selected.

The waves were selected according to their importance in real

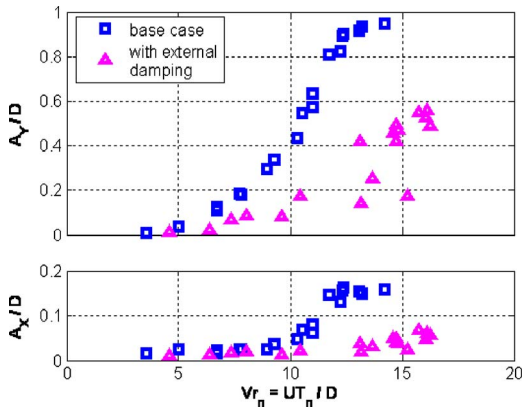

Fig. 35 Variation of the nondimensional amplitudes as a function of the reduced velocity for the 0-deg incidence with external damping

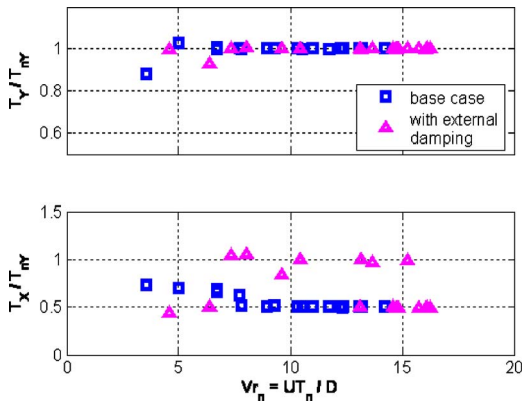

Fig. 36 Variation of the nondimensional periods as a function of the reduced velocity for the 0-deg incidence with external damping

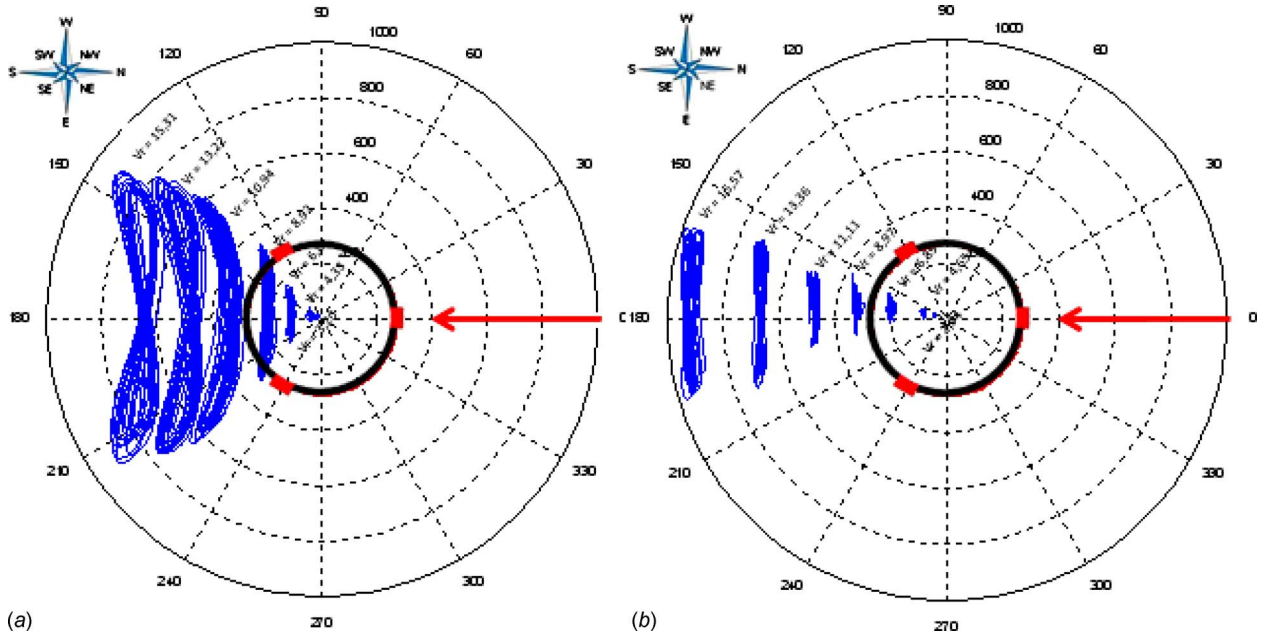

Fig. 37 Motions on the *XY* plane (in-line and cross-flow) for the 0-deg incidence; (*a*) without and (*b*) with the presence of external damping (risers)

scale and to the capacity of the IPT basin to generate these waves, as well as to the linearity of the waves (steepness of 4%, at most). The selected waves are presented in Table 5.The periods were corrected in order to match the target value, as there is a target velocity between the wave front and the model.

Figures 40 and 41 present nondimensional amplitudes and periods as a function of reduced velocity. If the coexistence with waves seems to indicate a contribution to VIM mitigation, it also shows that it happens only under severe heave motions (see Fig. 42). This is another result that deserves further investigation, mainly by using a larger wave spectrum, including irregular conditions.

In terms of T_y/T_{ny} and T_x/T_{ny}, it is noted that, even in the presence of waves, it is possible to identify values proportional to the natural period in the transverse direction in still waters. An exception is made for motions in the in-line direction for $Vr_n < 10$, where the presence of waves causes response periods due to the VIM in the range of $0.5 < T_x/T_{ny} < 1.0$.

Another interesting aspect comes from the comparison between the *XY* plane trajectories. Therefore, comparing the results in Fig. 15 (without the incidence of waves) with the results in Fig. 43 (with waves and current), it is possible to identify the mitigation effect of this environmental agent.

Figure 44 shows the drag coefficient results for tests with the coexistence of waves and current. The drag forces (medium and dynamic) increase due to the effect of a complementary dissipation force as the wave periods approximate the heave motion natural period.

The results of C_L with simultaneous wave presence, Fig. 45,

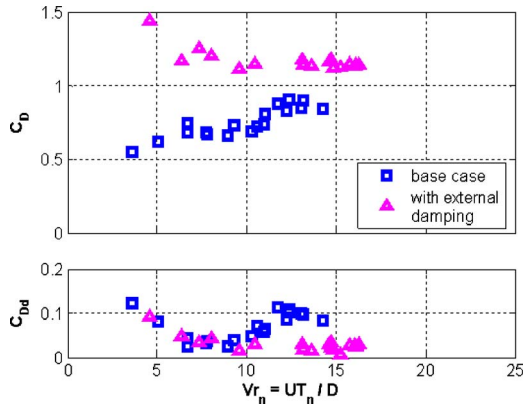

Fig. 38 Variation of drag coefficients as a function of reduced velocities for the 0-deg incidence with external damping

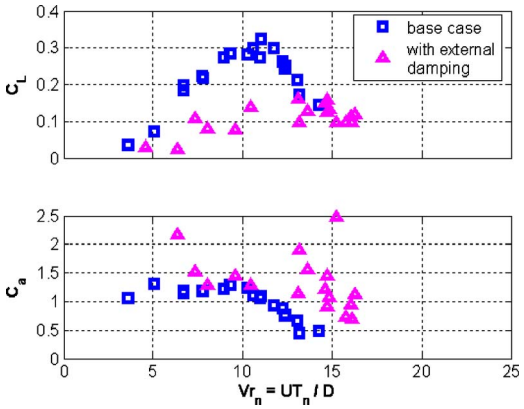

Fig. 39 Variation of the lift coefficient (C_L) above, and the added (C_a) below, as a function of the reduced velocity for the 0-deg incidence with external damping

Table 5 Regular waves selected for simultaneous VIM-wave presence (real scale)

Regular waves	Period, T (s)	Height, H (m)
Wave 1	14	4.00
Wave 2	16	5.22
Wave 3	18	6.88

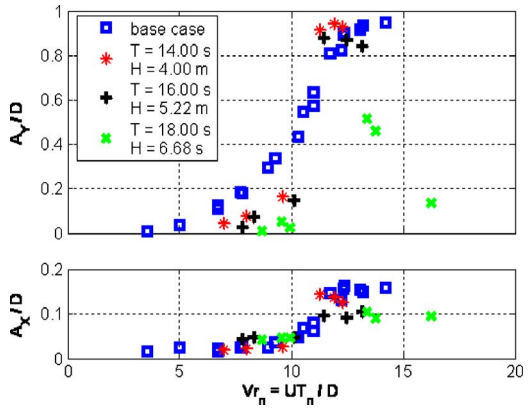

Fig. 40 Variation of the nondimensional amplitudes as a function of reduced velocity for the 0-deg incidence with simultaneous waves present

display a consistent behavior, presenting smaller values than the tests without waves; the simultaneous waves and currents are thus a mitigation effect of the VIM phenomenon.

Another important finding, which might be the key to the mitigation mechanism due to waves, is the increase in added mass when the period of the waves is near the heave natural period. There is, however, a large dispersion in the added-mass coefficient results, which may be due to the indirect measurement process (a difficult procedure under such conditions).

4.5 Tests With a Change in the Draft. Within all investigated aspects, this is the most effective in attenuating VIM. The results compare the MonoBR in operational draft ($L/D=0.39$) and

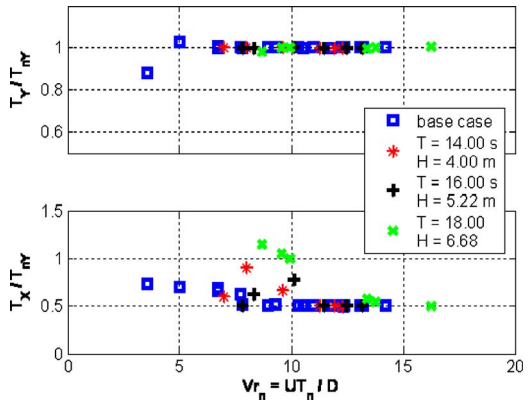

Fig. 41 Variation of the nondimensional periods as a function of the reduced velocity for the 0-deg incidence with simultaneous waves present

in light weight draft ($L/D=0.21$). Figures 46 and 47 show nondimensional motion amplitudes and periods, respectively, both for 0-deg incidence. A complete attenuation of VIM is noted in the results. The *XY* plane trajectory, Fig. 48, corroborates the above.

Concerning the forces, Figs. 49 and 50 show the absence of motions, where all the coefficients are coherent: $C_D \cong 0.75$, $C_{Dd} \cong 0$, $C_L \cong 0$, and $C_a \cong 1$.

5 General Conclusions

The following conclusions can be drawn based on the results presented previously.

1. The heading showed to be decisive in the VIM response of the platform. The 0-deg incidence, characterized by having one fairlead in front of the model, showed to be the critical situation, with the largest motion amplitudes. The 180-deg incidence, characterized by two fairleads in front of the model, was the second largest in motion amplitudes.
2. The 45-deg, 135-deg, and 315-deg incidences indicated to be less severely responsive, presenting occasional lack of symmetry. Such conditions are, however, still capable of damaging risers and mooring lines; see, for example, Ref. [27] that presented the importance of the VIM for studying fatigue analysis in risers.
3. Coexistence with waves proved to be very important in attenuating VIM, mainly in cases in which characteristic periods of the waves were close to the natural heave period of the MonoBR. Complementary studies with other regular waves and also sea conditions are necessary to strengthen this conclusion.
4. Albeit very efficient in experimental works previously conducted with the MonoGoM platform, see Ref. [3], the spoiler plates did not perform as well as expected in suppressing VIM on the MonoBR. Such behavior may be related to the need of a more detailed study concerning the placement geometry of the plates, motivating complementary studies with computational fluid dynamics (CFD).
5. Within all the aspects studied, the decrease in draft was the aspect that most contributed to the mitigation of VIM on the MonoBR. It is, therefore, important to take this into account the risers' and mooring lines' designs for systems subjected to VIM. Further tests using other drafts are suggested to consolidate this conclusion and, eventually, to define an emergency VIM draft.
6. The tests with risers showed that, besides modification of the emission pattern, their presence implies an increase in damping. Even though the added damping due to risers had not been scaled from the real system, studies demonstrated that their presence is very important for VIM.

As aforementioned, this work may serve as a database for calibrating numerical models for VIM prediction, as in Refs. [28–30].

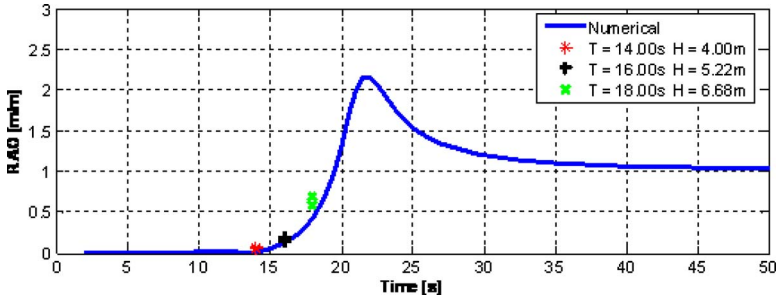

Fig. 42 Comparison between the heave response amplitude operator (RAO), numerically obtained and the experimental values obtained in the tests

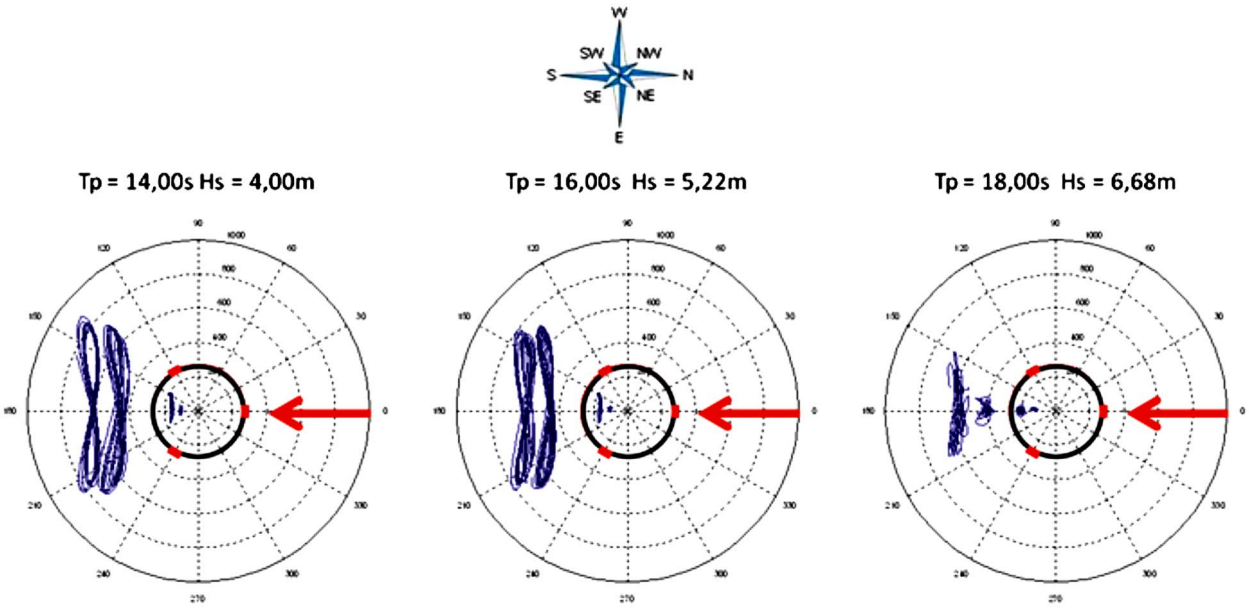

Fig. 43 Motions on the *XY* plane (in-line and cross-flow) for the 0-deg incidence, in three sea conditions

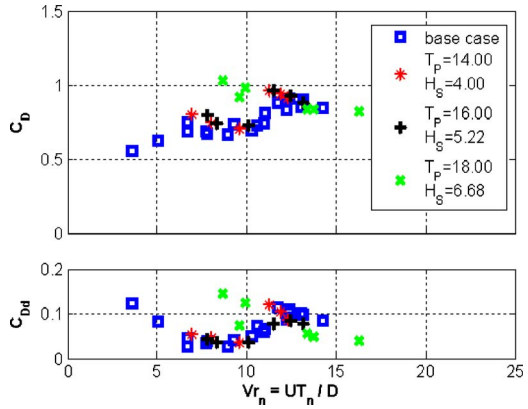

Fig. 44 Variation of drag coefficients as a function of reduced velocities for the 0-deg incidence with simultaneous waves present

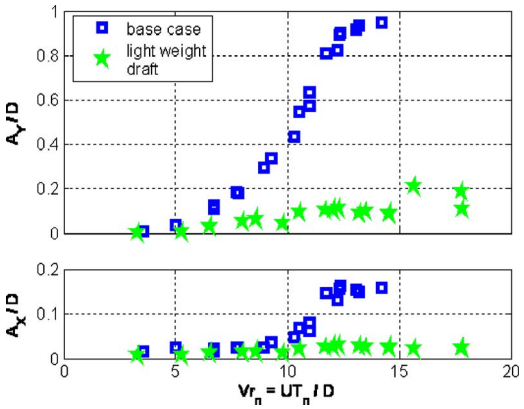

Fig. 46 Variation of the nondimensional amplitudes as a function of the reduced velocity for the 0-deg incidence varying draft

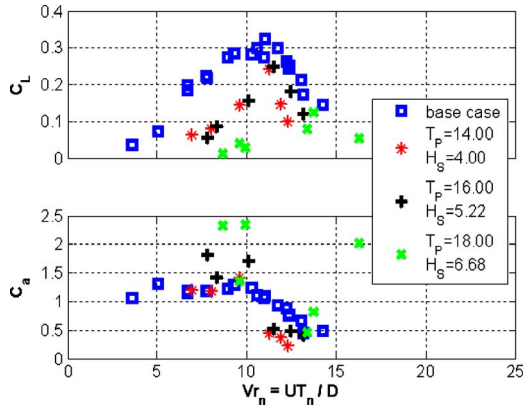

Fig. 45 Variation of the lift coefficient (C_L) above, and the added (C_a) below, as a function of the reduced velocity for the 0-deg incidence with simultaneous waves present

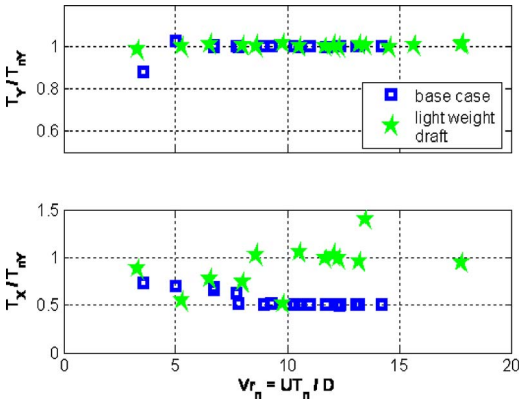

Fig. 47 Variation of the nondimensional periods as a function of the reduced velocity for the 0-deg incidence varying draft

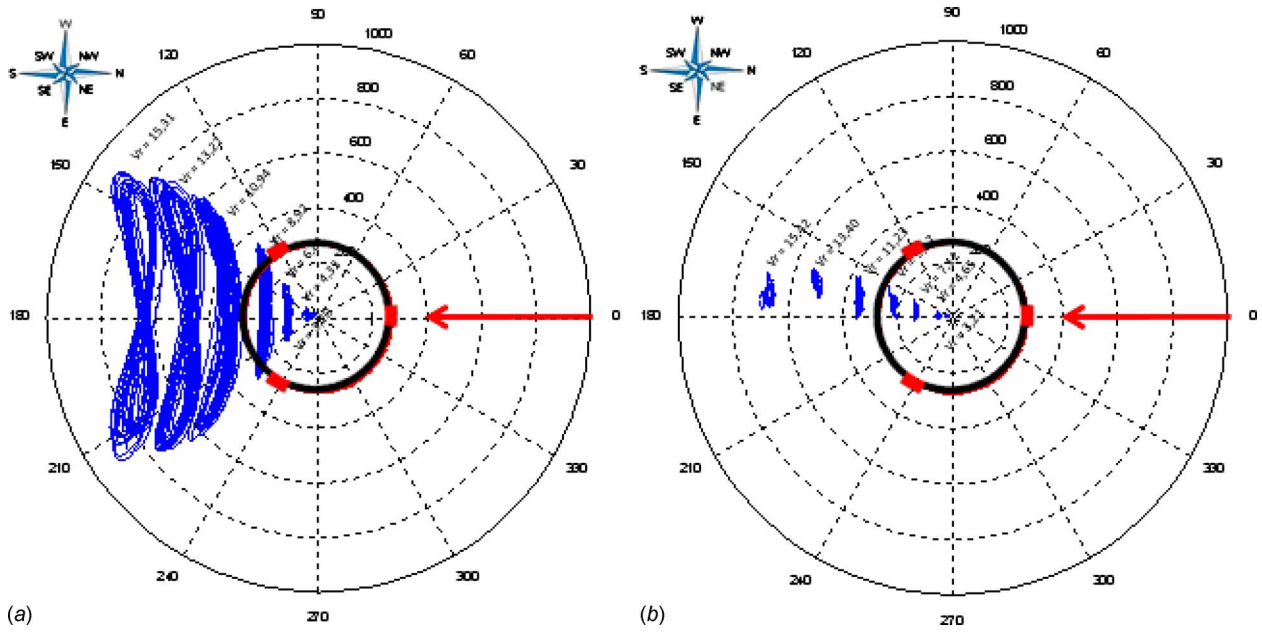

Fig. 48 Motions on the *XY* plane (in-line and cross-flow) for the 0-deg incidence; in two drafts: (*a*) operational and (*b*) light weight

Acknowledgment

The authors thank PETROBRAS, in particular, Eng. Dr. Elizabeth F.N. Siqueira, for their help in performing the tests. They also thank the IPT and Oceânica Offshore personnel, in particular, Fernando Faria and Marcos Cueva, for their efforts during the test campaign.

Nomenclature

ρ = fluid density
A_x/D = nondimensional amplitude motion in the in-line direction (20% highest peaks)
A_Y/D = nondimensional amplitude motion in the transverse direction (20% highest peaks)
C = structural damping
C_a = added-mass coefficient
C_D = mean drag coefficient
C_{Dd} = dynamic drag coefficient (oscillatory component)
C_L = lift coefficient
D = characteristic diameter of the platform
F_{Hx} = total hydrodynamic force in the in-line direction
F_{Hy} = total hydrodynamic force in the transverse direction
Fx = restoring force in the in-line direction
Fy = restoring force in the transverse direction
K_X = stiffness coefficient in the in-line direction
K_Y = stiffness coefficient in the transverse direction
k/D = nondimensional roughness
T_0 = natural period of the motion in the transverse direction in still water
T_{nY} = natural period of the motion in the transverse direction in the new offset position with current
T_x = in-line motion period
T_y = transverse motion period
U = flow velocity
Vr_n = reduced velocity (corrected)
X = X position of the center of gravity of the platform

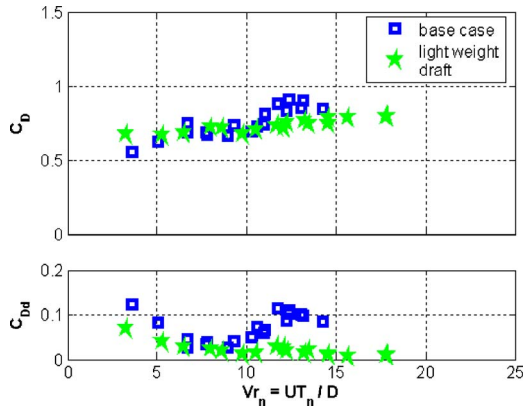

Fig. 49 Variation of drag coefficients as a function of reduced velocities for the 0-deg incidence varying draft

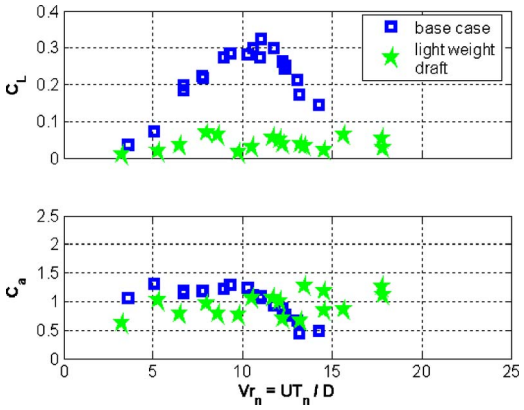

Fig. 50 Variation of the lift coefficient (C_L) above, and the added (C_a) below, as a function of the reduced velocity for the 0-deg incidence varying draft

x_{0i} = x position of the initial mooring point of the spring i

x_i = x position of the mooring point of the spring i at initial instant

Y = Y position of the center of gravity of the platform

y_{0i} = y position of the initial mooring point of the spring i

y_i = y position of the mooring point of the spring i at initial instant

Z = Z position of the center of gravity of the platform

z_{0i} = z position of the initial mooring point of the spring i

z_i = z position of the mooring point of the spring i at initial instant

References

[1] Gonçalves, R. T., Rosetti, G. F., Fujarra, A. L. C., Nishimoto, K., and Ferreira, M. D., 2009, "Relevant Aspects in Vortex-Induced Motions of Spar and Monocolumn Platforms: A Brief Overview," Proceedings of the 20th International Congress of Mechanical Engineering, Paper No. COB09-0581.

[2] Cueva, M., Fujarra, A. L. C., Nishimoto, K., Quadrante, L., and Costa, A., 2006, "Vortex Induced Motion: Model Testing of a Monocolumn Floater," Proceedings of the 25th International Conference on Offshore Mechanics and Arctic Engineering, Paper No. OMAE2006-92167.

[3] Gonçalves, R. T., Fujarra, A. L. C., Rosetti, G. F., Nishimoto, K., Cueva, M., and Siqueira, E. F. N., 2009, "Vortex-Induced Motion of a Monocolumn Platform: New Analysis and a Comparative Study," Proceedings of the 28th International Conference on Ocean, Offshore and Arctic Engineering, Paper No. OMAE2009-79378.

[4] Matsumoto, F. T., Gonçalves, R. T., Malta, E. B., Medeiros, H. F., Nishimoto, K., and Masetti, I. Q., 2008, "The Influence at Vertical First Order Motions Using a Appendages in a Monocolumn Platform," Proceedings of the 27th International Conference on Offshore Mechanics and Arctic Engineering, Paper No. OMAE2008-57410.

[5] Allen, D., and Henning, D., 2001, "Surface Roughness Effects on Vortex-Induced Vibration of Cylindrical Structures at Critical and Supercritical Reynolds Numbers," Proceedings of the Offshore Technology Conference, Paper No. OTC2001-13302.

[6] van Dijk, R. R., Magee, A., Perryman, S., and Gebara, J., 2003, "Model Test Experience on Vortex Induced Vibrations of Truss Spars," Proceedings of the Offshore Technology Conference, Paper No. OTC2003-15242.

[7] Yung, T. W., Sandström, R. E., Slocum, S. T., and Ding, J. Z., 2003, "Advances in Prediction of VIV on Spar Hulls," Deep Offshore Technology Conference, Marseilles, France, pp. 12–21.

[8] Irani, M., and Finn, L., 2004, "Model Testing for Vortex Induced Motions of Spar Platforms," Proceedings of the 23rd International Conference on Offshore Mechanics and Arctic Engineering, Paper No. OMAE2004-51315.

[9] Finnigan, T., and Roddier, D., 2007, "Spar VIM Model Tests at Supercritical Reynolds Numbers," Proceedings of the 26th International Conference on Offshore Mechanics and Arctic Engineering, Paper No. OMAE2007-29160.

[10] Huang, K., Chen, X., and Kwan, C. T., 2003, "The Impact of Vortex-Induced Motions on Mooring System Design for Spar-Based Installations," Proceedings of the Offshore Technology Conference, Paper No. OTC2003-15245.

[11] Roddier, D., Finnigan, T., and Liapis, S., 2009, "Influence of the Reynolds Number on Spar Vortex Induced Motions (VIM): Multiple Scale Model Test Comparisons," Proceedings of the 28th International Conference on Ocean, Offshore and Arctic Engineering, Paper No. OMAE2009-79991.

[12] Finn, L. D., Maher, J. V., and Gupta, H., 2003, "The Cell Spar and Vortex Induced Vibrations," Proceedings of the Offshore Technology Conference, Paper No. OTC2003-15244.

[13] Irani, M., and Finn, L., 2005, "Improved Strake Design for Vortex Induced Motions of Spar Platforms," Proceedings of the 24th International Conference on Offshore Mechanics and Arctic Engineering, Paper No. OMAE2005-67384.

[14] Finningan, T., Irani, M., and van Dijk, R. R., 2005, "Truss Spar VIM in Waves and Currents," Proceedings of the 24th International Conference on Offshore Mechanics and Arctic Engineering, Paper No. OMAE2005-67054.

[15] Yung, T. W., Sandström, R. E., Slocum, S. T., Ding, J. Z., and Lokken, R. T., 2004, "Advancement of Spar VIV Prediction," Proceedings of the Offshore Technology Conference, Paper No. OTC2003-1634.

[16] Fujarra, A., Pesce, C., Nishimoto, K., Cueva, M., and Faria, F., 2007, "Non-Stationary VIM of Two Mono-Column Oil Production Platforms," Proceedings of the Fifth Conference on Bluff Body Wakes and Vortex-Induced Vibrations—BBVIV, Costa do Sauipe, Bahia, Brazil, pp. 12–15.

[17] Sarpkaya, T., 2004, "A Critical Review of Intrinsic Nature of Vortex-Induced Vibrations," J. Fluids Struct., **19**, pp. 389–447.

[18] Vikestad, K., Vandiver, J. K., and Larsen, C. M., 2000, "Added Mass and Oscillation Frequency for a Circular Cylinder Subjected to Vortex-Induced Vibrations and External Disturbance," J. Fluids Struct., **14**, pp. 1071–1088.

[19] Khalak, A., and Williamson, C. H. K., 1999, "Motions, Forces and Mode Transitions in Vortex-Induced Vibrations at Low Mass-Damping," J. Fluids Struct., **13**, pp. 813–851.

[20] Fujarra, A. L. C., and Pesce, C. P., 2002, "Added Mass of an Elastically Mounted Rigid Cylinder in Water Subjected to Vortex-Induced Vibrations," Proceedings of the 21st International Conference on Offshore Mechanics and Arctic Engineering, Oslo, Norway, Paper No. OMAE2002-28375.

[21] Jauvtis, N., and Williamson, C. H. K., 2003, "Vortex-Induced Vibration of a Cylinder With Two Degrees of Freedom," J. Fluids Struct., **17**, pp. 1035–1042.

[22] Williamson, C. H. K., and Jauvtis, N., 2004, "A High-Amplitude 2T Mode of Vortex-Induced Vibration for a Light Body in *XY* Motion," Eur. J. Mech. B/Fluids, **23**, pp. 107–114.

[23] Stappenbelt, B., and Lalji, F., 2008, "Vortex-Induced Vibration Super-Upper Response Branch Boundaries," Int. J. Offshore Polar Eng., **18**, pp. 99–105.

[24] Blevins, R. D., and Coughran, C. S., 2009, "Experimental Investigation of Vortex-Induced Vibration in One and Two Dimensions With Variable Mass, Damping, and Reynolds Number," ASME J. Fluids Eng., **131**(10), p. 101202.

[25] Gopalkrishnan, R., 1993, "Vortex Induced Forces on Oscillating Bluff Cylinders," Ph.D. thesis, MIT, Cambridge, MA.

[26] Chakrabarti, S. K., 1994, *Offshore Structure Modeling*, World Scientific, Singapore.

[27] Sagrilo, L. V. S., Siqueira, M. Q., Lacerda, T. A. G., Ellwanger, G. B., Lima, E. C. P., and Siqueira, E. F. N., 2009, "VIM and Wave-Frequency Fatigue Damage Analysis for SCRs Connected to Monocolumn Platforms," Proceedings of the 28th International Conference on Ocean, Offshore and Arctic Engineering, Paper No. OMAE2009-79431.

[28] Lacerda, T. A. G., Ellwanger, G. B., Siqueira, M. Q., and Siqueira, E. F. N., 2008, "Time Domain Methodology for Vortex-Induced Motion Analysis in Monocolumn Platform," Proceedings of the 28th International Conference on Ocean, Offshore and Arctic Engineering, Paper No. OMAE2009-79806.

[29] Rosetti, G. F., Gonçalves, R. T., Fujarra, A. L. C., Nishimoto, K., and Ferreira, M. D., 2009, "A Phenomenological Model for Vortex-Induced Motions of the Monocolumn Platform and Comparison With Experiments," Proceedings of the 28th International Conference on Ocean, Offshore and Arctic Engineering, Paper No. OMAE2009-79431.

[30] Rosetti, G. F., Gonçalves, R. T., Fujarra, A. L. C., Nishimoto, K., and Ferreira, M. D., 2009, "Parametric Analysis of a Phenomenological Model for Vortex-induced Motions of Monocolumn Platforms," Proceedings of the 20th International Congress of Mechanical Engineering, Paper No. COB09-1097.

[31] van Dijk, R. R., Voogt, A., Fourchy, P., and Mirza, S., 2003, "The Effect of Mooring System and Shared Currents on Vortex Induced Motions of Truss Spars," Proceedings of the 22nd International Conference on Offshore Mechanics and Arctic Engineering, Paper No. OMAE2003-37151.